

A Compact Low-level RF Control System for Advanced Concept Compact Electron Linear Accelerator

C. Liu,¹ L. Ruckman,¹ R. Herbst,¹ B. Hong,¹ Z. Li,¹ K. Kim,¹ D. Amirari,² R. Agustsson,² J. Einstein-Curtis,³ M. Kilpatrick,³ J. Edelen,³ E. Nanni,¹ S. Tantawi,¹ and M. Kemp¹

¹SLAC National Accelerator Laboratory, Menlo Park, California, USA.

²RadiaBeam Technologies LLC, Santa Monica, USA.

³RadiaSoft LLC, Boulder, USA.

(*Electronic mail: chaoliu@slac.stanford.edu)

(Dated: 18 February 2025, The following article has been submitted to Review of Scientific Instruments by the AIP.)

A compact low-level RF (LLRF) control system based on RF system-on-chip (RFSoc) technology has been designed for the Advanced Concept Compact Electron Linear-accelerator (ACCEL) program, which has challenging requirements in both RF performance and size, weight and power consumption (SWaP). The compact LLRF solution employs the direct RF sampling technique of RFSoc, which samples the RF signals directly without any analogue up and down conversion. Compared with the conventional heterodyne based architecture used for LLRF system of linear accelerator (LINAC), the elimination of analogue mixers can significantly reduce the size and weight of the system, especially with LINAC requires a larger number of RF channels. Based on the requirements of ACCEL, a prototype LLRF platform has been developed, and the control schemes have been proposed. The prototype LLRF system demonstrated magnitude and phase fluctuation levels below 1% and 1° on the flat top of a 2 μs RF pulse. The LLRF control schemes proposed for ACCEL are implemented with a prototype hardware platform. This paper will introduce the new compact LLRF solution and summarize a selection of experimental test results of the prototype itself and with the accelerating structure cavities designed for ACCEL.

I. INTRODUCTION

The Advanced Concept Compact Electron Linear-accelerator (ACCEL) program aims to develop a high-power compact, rugged linear accelerator that can be easily transported and deployed in the field. The most critical and challenging requirement of the ACCEL is size, weight and power consumption (SWaP) of the linear accelerator (LINAC)¹. All the RF components of ACCEL, including the RF source, amplification, acceleration structure and low-level RF (LLRF), have been designed to achieve high RF power with stringent SWaP requirements. In this paper, the prototype compact LLRF system for ACCEL, including the hardware platform and control schemes, will be introduced and discussed.

The ACCEL system has been designed to operate in C-band around 5.712 GHz. The accelerating structure has 26 pairs of cavities and with each pairing sharing a single RF input and two RF monitors. With conventional LLRF system with heterodyne based architecture, at least 78 analogue up and down mixing circuits with discrete data converters would be required. The size and weight of the LLRF hardware will be substantial after including the field programmable gate array (FPGA) and processing system (PS) for control and interfacing. The compact LLRF system for ACCEL has been designed based on the RF system-on-chip (RFSoc) device family from AMD Xilinx. The RFSoc device integrates RF data converters, FPGA and PS, which are the essential components of a LLRF system. The integrated data converters in RFSoc devices offer higher order Nyquist zone sampling, which enable the C-band RF signals to be sampled or generated directly without analogue mixing. The RFSoc device selected for the compact LLRF, AMD Xilinx Zynq UltraScale+ RFSoc Gen

3 ZU49DR, has 16 RF analogue to digital converters (ADCs) with maximum RF input frequency of 6 GHz and a maximum sampling rate of 2.5 GHz and 16 RF digital to analogue data converters (DACs) with a maximum sampling rate of 9.85 GHz². The LLRF system for the complete ACCEL structure can be realized with 4 RFSoc devices with minimum other electronics. The high integration level of the RFSocs offers substantial benefits in the overall SWaP of ACCEL.

The RFSoc technology has been widely used in research and development of control and readout platforms for a range of physics experiments at SLAC National Accelerator Laboratory and other institutes we collaborate with³⁻⁸. The LLRF for the cool cooper collider (C³), which also operates in C-band, has been prototyped based on an RFSoc device in the same family as part of the road map for C³ R&D⁹⁻¹¹. The initial RF performance evaluation of the LLRF for C³ with a solid state amplifier (SSA) demonstrated magnitude and phase fluctuation levels within 1 s are 0.34 % and 0.37° respectively¹², which is considerably better than the 1% and 1° requirements for ACCEL. In¹³, the next generation LLRF (NG-LLRF) platform based on RFSoc developed at SLAC has been introduced. The NG-LLRF platform demonstrated that it can drive and measure a high-power test setup with high precision. The compact LLRF system for ACCEL has been designed and implemented based on configuration optimization and performance characterization exercises performed for RFSocs with the other LLRF systems of LINACs and other physics experiments. In Section II, the architecture of the prototype compact LLRF system, including hardware, firmware and software, will be introduced.

An LLRF system typically employs a pulse-to-pulse feedback loop to stabilize the RF field in an accelerating structure¹⁴. The pulse-to-pulse magnitude and phase control scheme proposed will be described in section III C. Due

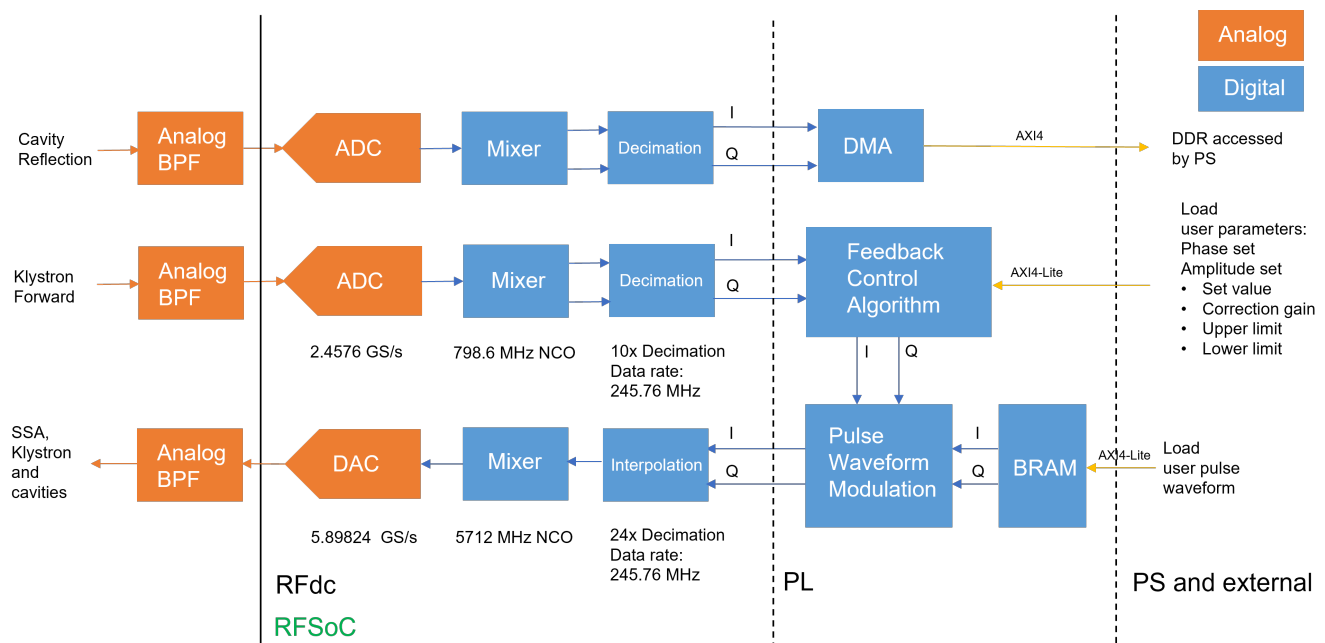


FIG. 1. The block diagram of the compact LLRF platform designed for ACCEL. A band pass filter (BPF) is used to reject the noise outside of the frequency range of interest. Data is transferred to the processing platform using direct memory access (DMA), which provides the high bandwidth access between different interfaces. Custom waveforms are stored in on-chip block random access memory (BRAM) to allow for custom pulse shapes.

to the special operating conditions of ACCEL, more control schemes are required. One of the design requirements of ACCEL is to operate in a wide temperature range without temperature stabilization for the accelerating structure. The resonant frequency of the accelerating structure can drift with the temperature substantially, which can affect the RF power injection to the structure. We have designed an RF frequency tuning scheme to track the resonance of structure cavities and change the RF frequency accordingly. The RF frequency tuning scheme will be described in Section III A. The ACCEL system is designed to be operated with an electron bunch train within an RF pulse, which require the phase and magnitude to be stable within each pulse. The scheme proposed to control magnitude and phase within the pulse will be described in Section III B.

The compact LLRF prototype has been tested at some critical stages of the development. The first test with the prototype has been performed is the direct loopback test with platform and the fluctuation levels of the loopback setup define the highest stability level of entire control system. The test results of loopback test setup will be summarized in Section IV A. The RF frequency tuning scheme has been implemented and tested with the ACCEL structure cavities. The RF signal before and after the RF frequency has been tuned to the resonance of the accelerating structure will be demonstrated and discussed in Section IV B. A prototype section of the compact LLRF system has also been tested with the high-power C-band test facility with a water load and a selection of the test results will be summarized in Section IV C.

II. COMPACT LLRF CONTROL HARDWARE PLATFORM

The prototype compact LLRF system for ACCEL has been developed based on the ZCU216 evaluation board, which carries an RFSoc Gen 3 ZU49DR device. A block diagram for the platform is shown in Figure 1. The solid line in Figure 1 defines the boundary between the RFSoc and the external components and signals. Within the RFSoc, the system implementation has been divided to three parts separate by the dashed lines: the RF data converter (RFdc), the programmable logic (PL) and the processing system (PS). The mixers and decimation or interpolation blocks before or after the data converter are integrated as a part of RFdc and each of the chain is named as a ‘datapath’. The datapaths for the data converters can be configured independently from each other.

For each pair of the ACCEL cavities, there are two RF signals to be measured and used for control and monitoring purposes, which are the klystron forward signal and cavity reflection signal. As Figure 1 shows, the RF signals are filtered with a band-pass filter and then sampled directly by the integrated ADCs in RFSoc at 2.4576 giga samples per second (GSPS). The digitized signal is then down converted to 798.6 MHz, which is the image of 5.712 GHz in the first Nyquist zone. The base-band signal in in-phase (I) and quadrature (Q) components are decimated by a factor of 10. Therefore, the bandwidth of the RF measurement chain in this case is 245.76 MHz. The bandwidth can be adjusted for future requirement by using a different decimation factor. The device uses digital finite impulse response (FIR) filters to reject high frequency noise as a part of the decimation process.

For the ACCEL structure design, there are no probes in the cavity structure. The cavity reflection is the only signal that carries information for the field inside the structure. In this version of the prototype, the IQ components of the cavity reflection signal in streaming format has converted to memory-mapped format and written to the DDR, which is outside of RFSoc chip. Data can then be accessed by the PS and sent to a server or processed locally on the PS. For the experiments in this paper, the data are sent to a server via Ethernet for further processing.

The down-converted klystron forward signal in IQ format is streamed to the feedback control algorithm firmware block. The user input parameters from the software layer are loaded to the firmware block via registers. Based on the IQ components and user input parameters, the control block calculates the updated IQ pair that compensate for the pulse-to-pulse fluctuation in phase and magnitude levels. The user can load a custom waveform via software, otherwise the default square wave will be used. The waveform is modulated with the updated IQ in the modulation block, which generates the updated base-band pulse. The DAC datapath interpolates the base-band pulse first and then up mixes with the digital values from the numerical controlled oscillator (NCO). The digital up conversion frequency can also be controlled via software. The DAC decodes and generates the updated RF pulse with a sample rate of 5.89824 GHz and drives the entire structure.

III. LLRF CONTROL SCHEMES

The ACCEL LLRF control system has been divided into three main parts based on the requirements. The control schemes proposed are designed to be performed in order: RF frequency control, followed by pulse shape control, and then the pulse-to-pulse phase and magnitude control feedback loop. The control schemes proposed are demonstrated in the form of flow charts in the following three subsections. In the flow charts, the orange blocks are planned be implemented in software and blue blocks to be implemented in firmware. The interface between the software and firmware will be defined in the Section III D.

A. RF frequency tuning

The targeted operation temperature range of ACCEL is from -40 to 85 °C. The resonant frequency of the accelerating changes by around 0.1 MHz per °C. Due to the limits in size and weight, there is no temperature stabilization mechanism for the accelerating structure of ACCEL and maintaining beam and beam energy is the priority of the program. Therefore, the RF frequency needs to be tuned according to the resonance frequency of the structure while operating.

Figure 2 shows the flow chart of RF frequency control flow. When the system is first switched on, the RF frequency control flow will be executed. The RF frequency will be coarsely set based on the reading of the temperature sensor and the

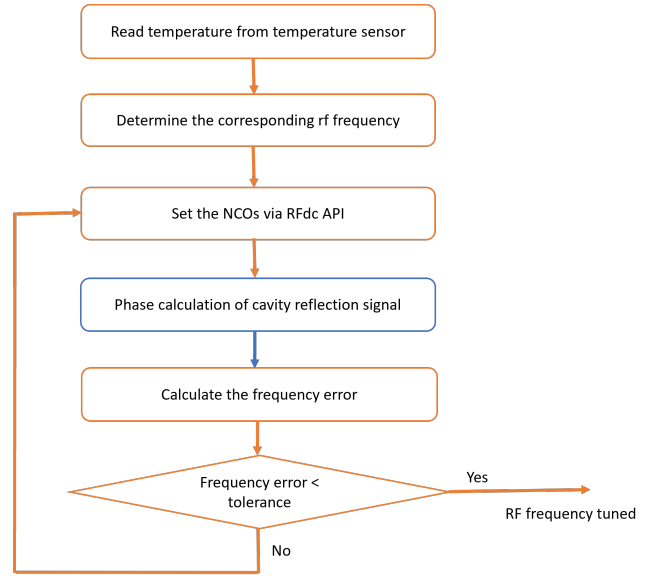


FIG. 2. The flow chart of the RF frequency tuning routine proposed for ACCEL LLRF system.

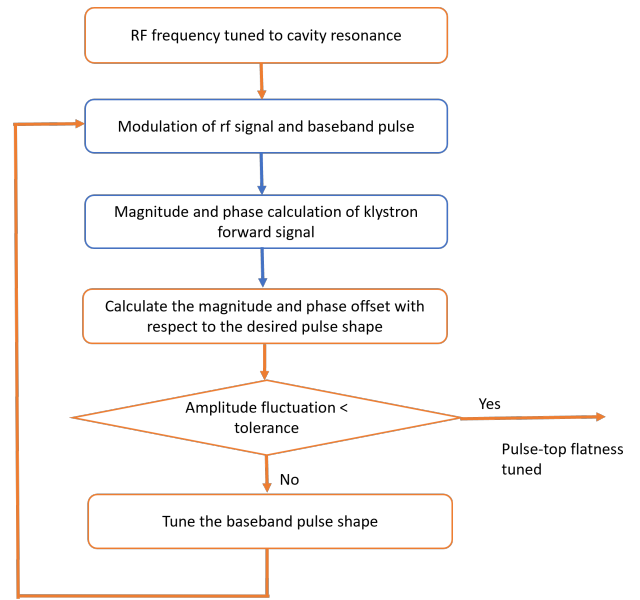


FIG. 3. The flow chart of the RF shape control routine proposed for the ACCEL LLRF system.

look up table of temperature verse RF frequency that is embedded in the software. With the coarse RF frequency tuning, a fraction of RF power should be able to be injected into the cavity and the energy stored in the structure will radiate at the resonant frequency of the structure after the RF pulse is off. The radiation can be captured by the cavity reflection coupler and the IQ samples of the cavity reflection signal from the ADC datapath is sent to software. Then the frequency error can be calculated based on the phase of the cavity reflection signal after the RF pulse is off and the calculation theory and experimental results will be elaborated in section IV B. The

updated RF frequency calculated by software is loaded to the data converter datapaths and changes the frequency of the sequence generated by the NCOs, which will ultimately update the RF frequency for both the ADCs and DACs. The process frequency correction can be executed in a controlled step size until the frequency error is below a desired value defined by the user. Based on the gradient of temperature change while operation, the frequency tuning loop can be executed at an adaptive rate.

B. RF pulse shape control

Figure 3 shows the flow chart of the pulse shape control scheme. After the RF frequency is set to the resonance of the accelerating structure by the RF frequency tuning loop, the pulse shape control flow will be executed. As there is no probe that measures the RF field in the structure directly and the RF field follows the klystron by design, the klystron forward signal is employed for RF pulse shape control. The magnitude and phase values of the klystron forward signal are sent to software to calculate the updated pulse shape that can compensate for any fluctuation within the pulse. In software, the updated pulse shape is calculated based on the variation between the desired and measured pulse shape to reduce the offset between them sample by sample. Then the updated base-band pulse shape in IQ format is loaded to the firmware and upconverted to drive the system for the following pulse. The procedure repeats until the standard deviations of magnitude and phase on flat top are below the desired levels. The pulse shape should be consistent after the compensation procedure is performed, so the pulse shape control may not required to be executed continuously after the first run. However, more development and test efforts are required to verify the optimal control routine and algorithm.

C. Pulse-to-pulse Magnitude and Phase Control

Measuring and stabilizing the magnitude and phase of the field in the accelerating structure is the primary objective for most of LLRF control systems of LINACs. Figure 4 shows the flow chart of phase and magnitude control we have proposed for ACCEL. After the RF frequency and pulse-top flatness are tuned to desired levels, the phase and magnitude feedback control loops will start operating. This control loop is also implemented by using the klystron forward signal. In firmware, the base-band klystron forward signal from ADC datapath will be processed with moving average with certain number of samples to improve the signal stability. The IQ components are converted to phase and magnitude values and the average values will be computed. The current average magnitude and phase values will be compared to the user defined values and then calculating for a new set of magnitude and phase values to approach the user defined values in the defined rates. The new set of magnitude and phase values are converted back to IQ format and modulated with the base-band pulse waveform. The up converted RF signal samples are finally clocked into

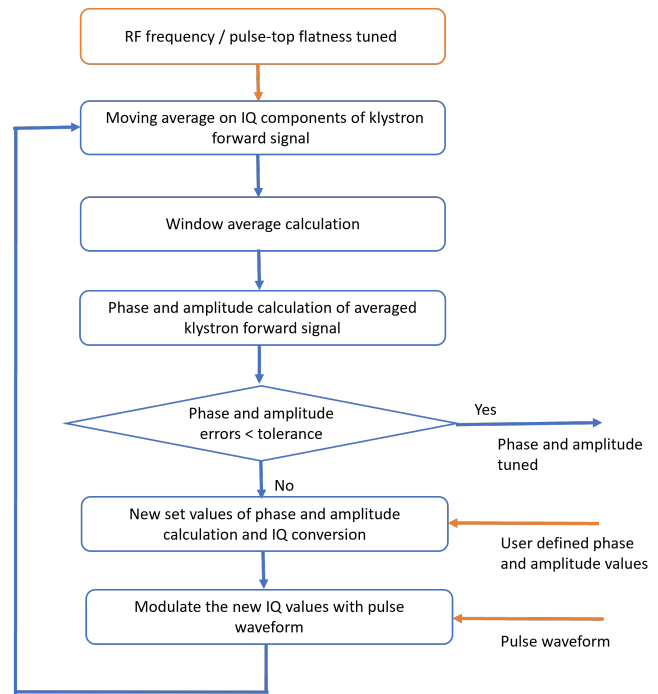


FIG. 4. The flow chart of the pulse-to-pulse magnitude and phase feedback control loop proposed for the ACCEL LLRF system.

the DAC to generate the updated RF pulse, which will be used as the drive of accelerating structure for the following pulse. The feedback loop runs continuously during operation to perform real-time pulse to pulse magnitude and phase correction. If the difference between the measurement and desired values are below a certain threshold, the values will not be changed for the following pulse. This is to minimize the instability introduced by the LLRF if the desired signal levels are already meeting operating requirements.

D. Interface between Firmware and Software

The data converter and firmware implemented in RFSoc is managed by a suite of software based on SLAC's Rogue architecture¹⁵, which provides the hardware abstraction layer and interface to higher level software. The low-level interface between the firmware and software is facilitated by a custom kernel driver that provides an interface to streaming data through a firmware DMA engine as well as providing an application programming interface (API) for reading and writing registers contained in the FPGA.

The interface for the communication between the hardware abstraction layer and the higher-level software is implemented with the Experimental Physics and Industrial Control System (EPICS) version 7 process variable access (pvAccess) variables¹⁶ while also having hooks for integration with other command protocols. Base-band samples will be presented as Numpy arrays of the appropriate data type and scalar variables are presented as their native type. The state control, state monitoring, and other interfaces between higher level control soft-

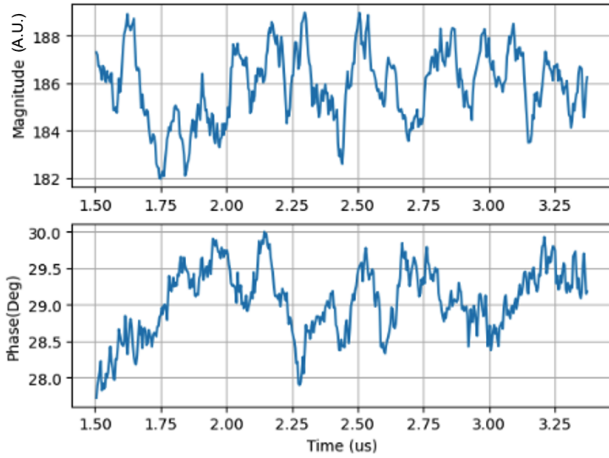


FIG. 5. The magnitude and phase fluctuation on a $2 \mu\text{s}$ pulse with DAC amplitude of 8000.

ware and the hardware abstraction layer will also occur over EPICS V7. A client interface is provided to access a debug interface directly to the firmware and associated support hardware. Additionally, the hardware abstraction layer facilitates streaming data for debugging purposes.

IV. EXPERIMENTAL TEST OF THE COMPACT LLRF PROTOTYPE FOR ACCEL

In the process of prototyping the compact LLRF for ACCEL, a range of experimental tests have been performed for performance evaluation and functional verification purposes. The test begins with the simplest loopback from the DAC to the ADC of the compact LLRF prototype and then test broadens to include the to higher power regime with solid state amplifier and klystron. The test results at different stages of the system or different parts of the system, which are important for the final implementation of the control schemes are summarized and analyzed in this section.

A. Loopback Test of the Compact LLRF Prototype

The direct loopback is a critical test of the compact LLRF system, as it can reveal the performance of the platform without relying on other test equipment. The loopback test can also expose functional defects and performance issues. The direct loopback tests for C-band LLRF system in different test conditions have been summarized in recent publications^{12,13}. We have performed a compressive direct loopback test, which demonstrated magnitude and phase fluctuation levels of 0.13% and 0.14° in 1s respectively with both ADC and DAC operating in the optimum input and output ranges. Further testing of magnitude and phase stability is ongoing and will be available in future publications. In¹², the loopback test with $1 \mu\text{s}$ pulse at 60 Hz with the a similar SSA

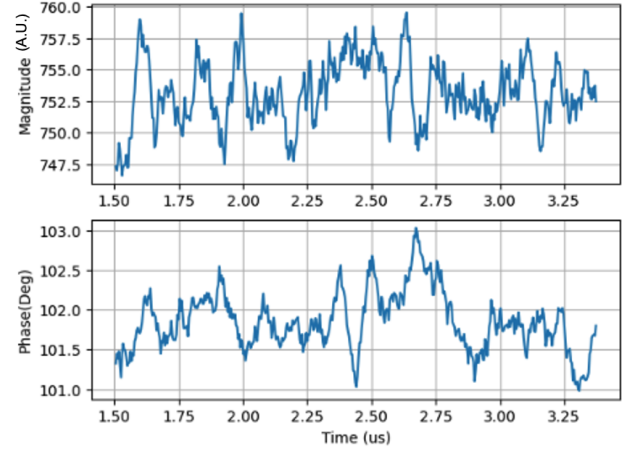


FIG. 6. The magnitude and phase fluctuation on a $2 \mu\text{s}$ pulse with DAC amplitude of 32000.¹²

and the ZCU216 evaluation board used for tests in this paper has delivered magnitude and phase fluctuation levels of 0.09% and 0.18° . The pulse-to-pulse evaluation results are significantly better than the $\pm 1\%$ and $\pm 1^\circ$ requirements for ACCEL, which means pulse-to-pulse feedback requirement is achievable with the compact LLRF platform. Due to the multi-bunch operation of ACCEL, the flatness of magnitude and phase within each pulse is also required to be $\pm 1\%$ and $\pm 1^\circ$. The targeted flat-top duration for each pulse is in 1 to 5 μs range.

In this case, flatness of the pulse top has been evaluated at two amplitude levels. The RF pulse used for this test is $2 \mu\text{s}$ at 60 Hz. As the RF pulses are generated by the DAC datapath, the magnitude of base-band pulse is used to denote the level of RF pulse, which named as ‘DAC amplitude’ in this case. The test has been performed at two different DAC amplitude levels, which are 8,000 and 32,000. The 32,000 DAC amplitude is close to the maximum value that can be used for the digital mixing in the pulse generation process. The RF pulse is generated by the DAC of the compact LLRF and then looped back to an ADC via BPFs. The ADC samples the RF pulse directly and IQ components after down conversion are recorded. In the post analysis, the data in IQ format has been converted to magnitude and phase format. The magnitude and phase values on the flat top of the two DAC amplitude levels are shown in Figure 5 and 6.

The average values of magnitude measured with DAC amplitude at 8000 and 32000 are approximately 186 and 752, which follows the desired linear trend. There is not obvious common drifts or oscillations for both magnitude and phase values at the two DAC amplitude levels. The magnitude fluctuation on the pulse top is measured by the percentage of standard deviation respect to average over the flat top. The fluctuation for 8,000 and 32,000 DAC amplitude levels are 0.8% and 0.34%. The phase fluctuation is directly measured with the standard deviation levels, which are 0.47° and 0.37° for the DAC levels of 8,000 and 32,000 respectively. Operating the DAC and ADC in higher range benefits the fluctuation

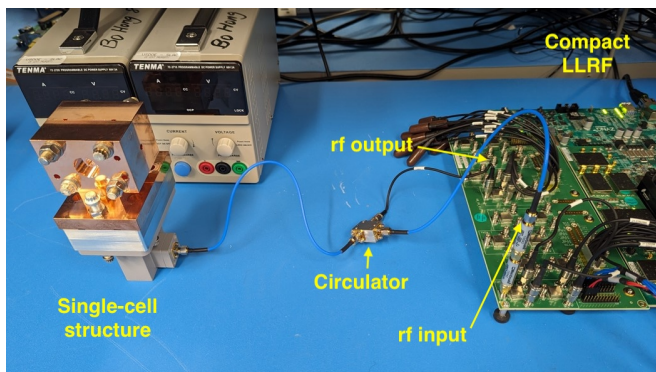


FIG. 7. The test setup of single-cell structure with the compact LLRF for ACCEL.

tuation levels for both magnitude and phase values within a single pulse. The amplification or attenuation levels in the final LLRF should be optimized with respect to the input and output ranges of ADCs and DACs. Even though the RF signal used in this test is on the lower side of the ADC, the flatness levels achieved are still considerably better than the 1% and 1° requirement. That indicates the compact LLRF prototype can generate and measure the RF pulses within the desired fluctuation level.

B. RF Frequency Tuning Scheme Tests

As introduced in Section III A, the wide operation range of ACCEL and the lack of temperature stabilization made an RF frequency tuning scheme necessary. In this section, the technique for fine frequency tuning will be presented and the tuning routine implemented will be tested with both single-cell and dual-cell ACCEL accelerating structures.

1. Single-cavity Structure Test

The first test of RF frequency tuning was performed with the simple test setup shown in Figure 7. The RF output of compact LLRF system generates RF pulses at 60 Hz. The RF pulses are injected to the single-cell structure, which is a prototype cavity for ACCEL, via a circulator. The circulator with bandwidth of 4 to 8 GHz, PACL1704000800A, manufactured by DBwave Technologies LLC has been used for this test. The circulator couples the reflected RF signal from the structure and the signal is connected to one of the RF input channels of the compact LLRF system. The cavity reflection signal is sampled directly by the ADC channel and down converted by the following datapath. The IQ samples collected are converted to magnitude and phase for analysis in this section.

For the first step, the test setup was driven by RF pulses with the RF frequency of 5.712 GHz and measured at the same RF frequency. The magnitude and phase values of the cavity reflection signal are shown in Figure 8. The magnitude of

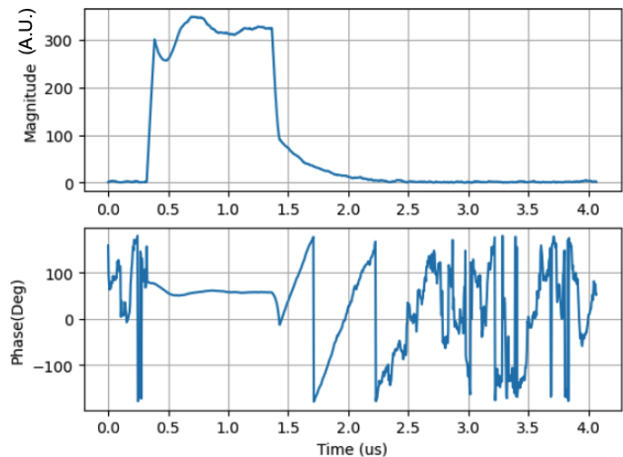


FIG. 8. The magnitude and phase values of cavity reflection signal before the RF frequency tuning.

the cavity signal has ripples after the initial rise and remains generally flat until the RF pulse is off. The reflection signal remains high over the pulse duration indicating that the RF power injected to the structure is almost fully reflected as a result of driving the system off the resonant frequency of the cavity. When the structure is driven off resonance within certain threshold, the structure will still be energized, but with an extremely low gain. The single-cell structure has been designed to resonate at 5.712 GHz, but machining errors and ambient temperature can introduce offsets to its resonance. The phase level of the reflection signal remains stable until the RF pulse is off and there is a steep linear ramp after the RF is off. The reflection after the RF pulse is off is dominated by the radiation from the structure cavity. The structure radiates the RF energy at its resonance frequency. When the RF frequency and the down conversion frequency are different, it will be reflected as a linear ramp on the phase level. The offset between the structure resonance and the operation RF frequency of the LLRF system can be calculated with Equation 1.

$$\Delta\omega = \frac{d\phi}{dt} \quad (1)$$

The phase values has been transferred to software and frequency offset has been computed with the slope of phase ramp after the RF is off. The resonant frequency of the single-cell structure computed by using Equation 1 is approximately 2.08 MHz higher than 5.712 GHz. Then the RF frequency of the LLRF has been adjusted to the resonance frequency of the cavity and the procedure above has been repeated. The magnitude and phase levels of the cavity reflection signal after frequency tuning are shown in Figure 9. The magnitude of the reflection ramps down after the first spike and that demonstrates the field filling process in the accelerating structure. The cavity reflection reaches the lowest magnitude when the filling process is completed. As there is no beam and the structure is overcoupled, the second peak on the magnitude of reflection is higher than the first one. The filling and dissipation

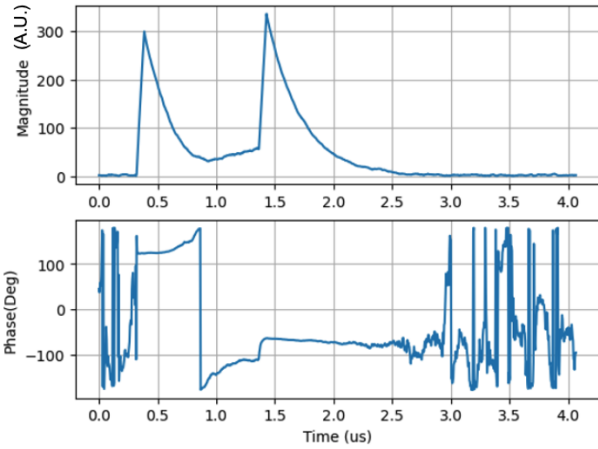


FIG. 9. The magnitude and phase values of cavity reflection signal after the RF frequency tuning.

processes also reflect on the phase level. The phase has been reversed when the structure is fully filled. The magnitude and phase level before the RF pulse is switched off shows that the RF signal can be successfully injected to the structure and established field to fill the structure.

After the RF pulse is off, the magnitude ramps down, which shows the stored RF power radiating and dissipating in the structure. The phase level remains almost flat after the pulse is off, which means the operation frequency of the LLRF is close to the resonance frequency of the structure. That signifies that the RF frequency tuning has been successful for the single-cell structure with a high precision.

2. Dual-cavity Structure Test

In the final design of ACCEL, the full accelerating structure will be composed by 26 dual-cell structures. After the RF frequency tuning scheme has been verified to be functional with the single-cell structure, the test has been extended to the dual-cell structure with a higher power SSA. Figure 10 shows the test setup with the dual-cavity structure. The RF pulse generated by the compact LLRF system is amplified by a low noise amplifier, as the output power of the compact LLRF is consider too low to drive the SSA. The SSA amplifies the resultant RF pulse again and the peak power is up to 300 W. The forward RF power is measured at the output of the SSA via a coupler. The output of the SSA is injected to a dual-cell structure via an adapter. The reflection signal is measured at the reflection port via a load and an adapter. Both the forward and reflection signals are attenuated and looped back via the RF input measurement channels.

Compared with the single-cell structure, the RF frequency tuning of the dual-cell structure is more complicated. As the two cells of the structure have different resonance frequencies due to the machining tolerance. The resonant frequencies of the cells are measured using the same method described in Section IV B 1 with one of the cells detuned. The measured

resonant frequencies of the two cells are differed by approximately 0.32 MHz. The resonance frequency for the one of the cell is then tuned close to the other cell by inserting a metal wire via the hole on the wall of structure. For the dual-cell structure in production, this step will be replaced by mechanical tuning before assembly.

After the resonance frequency of the two cells are tuned to a similar level, the RF frequency tuning scheme was tested. The test begins with RF pulse at RF frequency of 5.712 GHz and Figure 11 shows the magnitude and phase levels of the cavity reflection signal. The magnitude of the reflection oscillates with a slightly reducing magnitude after the initial rise, which indicates that the power is almost fully reflected and the structure has been energies with a extremely low gain. Then the magnitude level settle in about 0.6 μ s showing that no more power has been injected to the structure afterwards. While the pulse is on, the phase of the reflection remains in a stable level with some oscillation at early stage. After RF pulse is switched off, there is linear ramp on the phase level with steep slop. The resonant frequency computed for the for the dual-cell structure is around 7.5 MHz higher than 5.712 GHz.

The test was performed again after the operation RF frequency of the compact LLRF system is tuned to the structure resonant frequency and the magnitude and phase levels of the cavity reflection signal are shown in Figure 12. The magnitude of the reflection signal shows a different field filling process compared with the single-cell structure. The dual-cell structure has been designed to have a coupling factor (β) around 4.6 and the magnitude is expected to reach the minimum after the first peak in 100 ns. The magnitude of the cavity reflection shown in the figure reaches the minimum around 100 ns as the radiation from the cavity and reflection from the iris almost cancelled with each other. Then the structure cells are filled for about 500 ns until the reflection signal reaches an steady level. As the structure is designed to be overcoupled without the beam, the second peak after the RF is switched off is approximately 60 % higher than the first peak. The phase remains flat after the RF pulse is off, which indicates that the operating frequency of the prototype ACCEL compact LLRF is extremely close to the resonance of the dual-cell structure. This shows that the RF frequency tuning scheme of LLRF system can successfully measure the resonant frequency of the dual-cell accelerating structure and tune operating frequency to be aligned with the cavity resonance frequency.

C. Compact LLRF Prototype Tests with High-power Test Facility

The compact LLRF platform was tested at the C-band test facility at Radiabeam at higher power levels. The test was focused on investigating the fluctuation levels and patterns on the klystron forward signal, which is critical for the design and implementation of pulse shape control scheme. The C-band klystron is driven by the RF pulse generated by the RF output of the compact LLRF platform. Then the output RF power of klystron is coupled to the test bunker via a waveguide. For this test, the peak power generated by the klystron is 426 kW

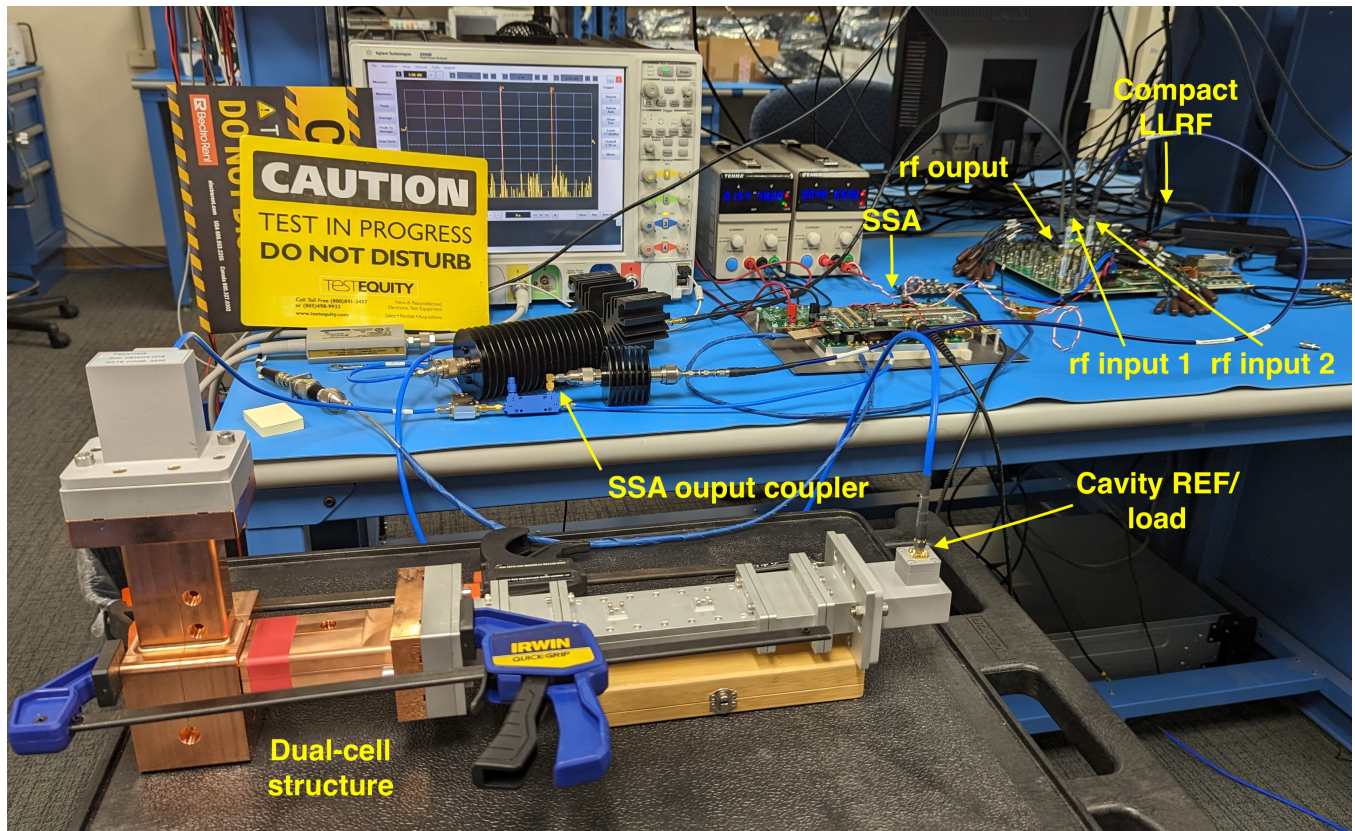


FIG. 10. The test setup of the two-cell structure with the SSA and the compact LLRF prototype.

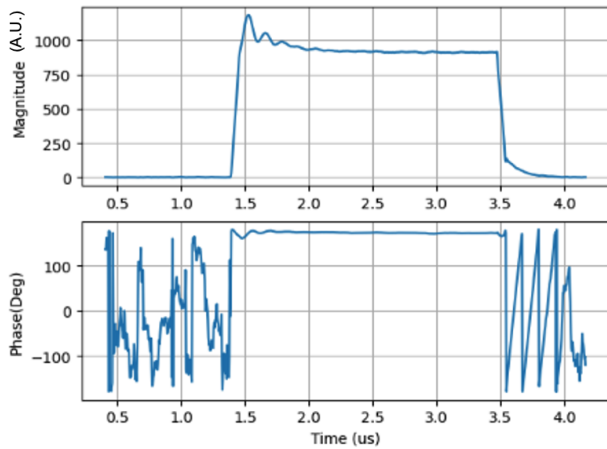


FIG. 11. The magnitude and phase values of the cavity reflection signal before the RF frequency tuning.

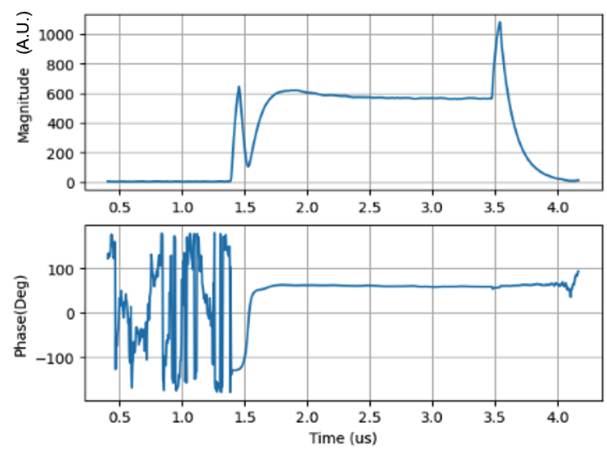


FIG. 12. The magnitude and phase values of cavity reflection signal after the RF frequency tuning.

and 199 kW is delivered to the load in the test bunker. Figure 13 shows the setup in the test bunker. The RF power from the waveguide is coupled to a water load via a power splitter and phase shifter (PSPS).

The RF power at the output of the klystron and the input of water load are measured with directional couplers. Figure 14 shows the magnitude and phase levels of the klystron forward

and load forward, which are labeled as 'klystron FWD' and 'Load' respectively. The magnitude of the first peak of the load forward signal is scaled to match the first peak of klystron forward signal. The magnitude and phase levels of the load follows the klystron forward power as expected and both have a ramp up about 100 ns after the first peak. The flat top with steady magnitude and phase is approximately 600 ns within

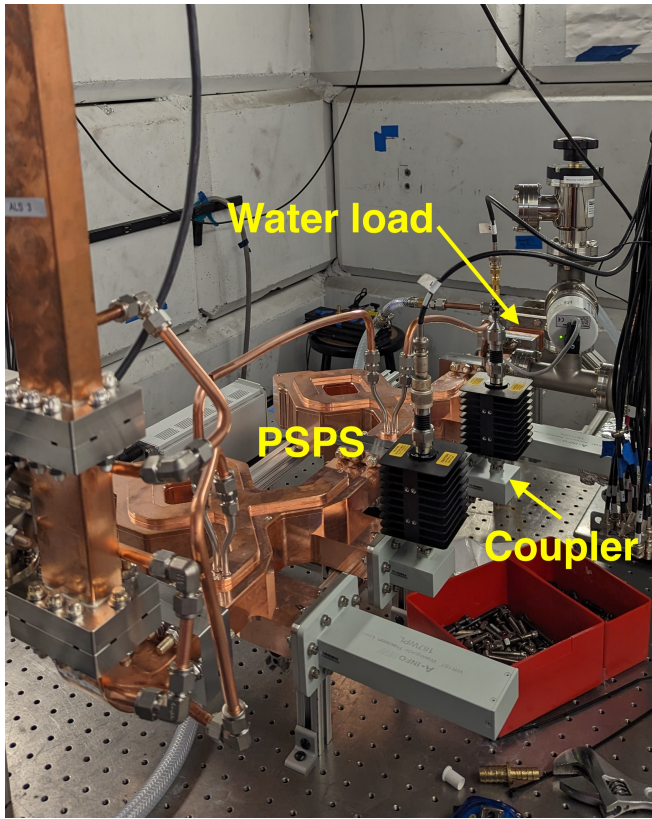


FIG. 13. The test setup of single-cell structure with the compact LLRF for ACCEL.

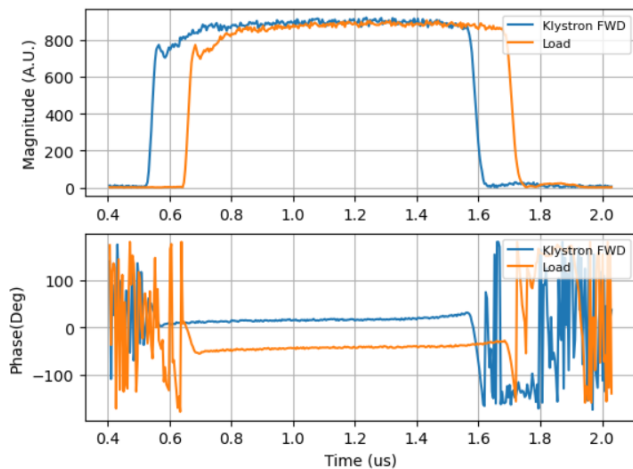


FIG. 14. The magnitude and phase of the klystron forward and load forward signal measured in high-power test.

the 1 μ s RF pulse.

The magnitude fluctuation is evaluated with the percentage of the standard deviation of the magnitude values in the 600 ns flat top with respect to the average magnitude in the period. The magnitude fluctuation levels for the klystron forward and load forward are 1.60 % and 1.51 % respectively. The phase fluctuation level is measured directly with the standard deviation

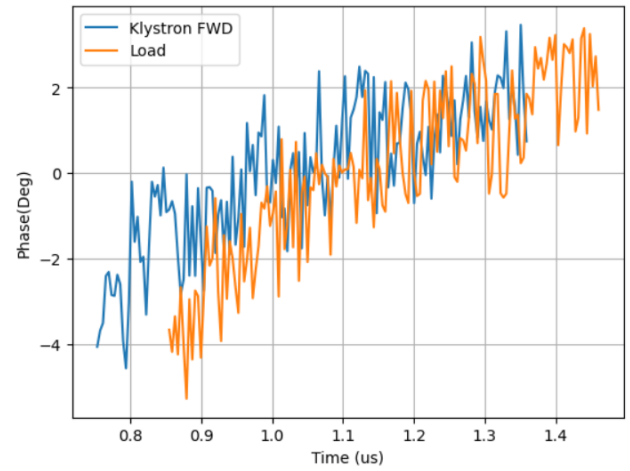


FIG. 15. The phase levels of the klystron forward and load forward signals on the 600 ns flat top measured in high-power test.

of the phase values on the flat top. The phase fluctuation levels for the klystron forward and load forward are 1.66° and 1.98° respectively. The magnitude and phase fluctuation levels at klystron forward and load forward are consistent, which means the RF power generated by the klystron has been successfully delivered to the load in the test bunker and RF signals are measured with high precision by the compact LLRF platform. The fluctuation levels for both magnitude and phase measured on the flat top are above the 1% and 1° requirement of ACCEL, which verified the necessity of pulse shape control scheme.

Figure 15 shows the phase levels of klystron forward and load forward signals on the 600 ns flat top. The average phase of each of the signals has been subtracted. There is a linear phase ramp start from approximately -4° and up to 3° until the end of the flat top on both of the signal. The ACCEL system requires flat top between 1 to 5 μ s, so the phase drift will be even more significant. The phase drift introduced by the klystron is far higher the ACCEL requirement. The drift need to be compensated by the pulse shape control scheme with phase modulation techniques. As the modulation of the compact LLRF is fully implemented in digital domain, the phase and magnitude modulation can be implemented with high flexibility. We have tested a similar RFSoc based LLRF with of several phase modulation schemes at high power regime. The high-power test demonstrated the capability of generating and measuring phase modulation schemes with high precision and the full results will be published in the near future.

V. CONCLUSION

A compact LLRF system prototype based on RFSoc technology has been designed and developed for the ACCEL program. Compared with conventional LLRF systems, the higher integration level and the direct RF sampling of RFSoc offers distinctive SWaP advantages for the compact LLRF system we proposed for ACCEL. Due to the special operation

and application requirements of ACCEL, additional control schemes, such as the automated RF frequency tuning and pulse shape control, are required. The initial control schemes proposed, including: the time sequence, the building blocks and the interface between software and firmware have been introduced. The hardware, firmware, and software of the compact LLRF platform has been designed, implemented and tested, with each block at different levels of completion. The development of the complete prototype will continue in the next phase of the project.

The prototype enabled a range of feasibility studies and experimental tests for different purposes. In the initial loopback test, the compact LLRF system demonstrated magnitude and phase fluctuation levels at 0.34% and 0.37° on the flat top of a 2 μ s RF pulse. The RF frequency tuning scheme test demonstrates the scheme can measure the resonant frequency of single-cell and dual-cell ACCEL accelerating structure prototypes and tune the operation RF frequency of the LLRF system with high precision. The field filling, reflecting and dissipation processes can be visualized on the reflection signal from the structure before and after the RF frequency is tuned.

The high-power test has been performed in the lower power regime of the klystron, which has a maximum peak power output of 50 MW. As the klystron was operated far below saturation, the RF power generated is less stable. The klystron forward and load forward measurements revealed fluctuation levels and drift patterns introduced by the the klystron. Those features will be a critical reference when implementing the full pulse shape control scheme.

There are a range of test and development tasks to be completed before the compact LLRF can be operated with all the control schemes required. The firmware building blocks of the pulse-to-pulse feedback control scheme have been implemented, but not yet tested in a full-firmware implementation. Due to the limits on the schedule, the high-power test has been performed at a relative low power level and without an ACCEL accelerating structure. A high-power test with the ACCEL structure and the compact LLRF platform should be performed in the next phase of the project.

ACKNOWLEDGMENT

The work of the authors is supported by the DARPA. The views, opinions and/or findings expressed are those of the authors and should not be interpreted as representing the official views or policies of the Department of Defense or the U.S. Government. The work of the authors is also partially supported by the U.S. Department of Energy under Contract No. DE-AC02-76SF00515.

DATA AVAILABILITY STATEMENT

The data underlying this article will be shared on reasonable request to the corresponding author.

- ¹DARPA, “Advanced concept compact electron linear-accelerator (accel),” Published on U.S. Department of Defense website <https://www.darpa.mil/program/advanced-concept-compact-electron-linear-accelerator>, (Accessed: 11 August 2024).
- ²AMD, “Amd zynq ultrascale+ rfsocs,” Published on AMD website <https://www.amd.com/en/products/adaptive-socs-and-fpgas/soc/zynq-ultrascale-plus-rfsoc.html>, (Accessed: 11 Feb 2025).
- ³C. Liu, M. E. Jones, and A. C. Taylor, “Characterizing the performance of high-speed data converters for rfsoc-based radio astronomy receivers,” *Monthly Notices of the Royal Astronomical Society* **501**, 5096–5104 (2021).
- ⁴C. Liu, M. E. Jones, and A. C. Taylor, “Development of general-purpose digital backend for single-dish centimetre and millimetre-wave telescopes,” in *2022 3rd URSI Atlantic and Asia Pacific Radio Science Meeting (AT-AP-RASC)* (IEEE, 2022) pp. 1–4.
- ⁵C. Liu, L. Ruckman, and R. Herbst, “Evaluating direct rf sampling performance for rfsoc-based radio-frequency astronomy receivers,” arXiv preprint arXiv:2309.08067 (2023).
- ⁶S. W. Henderson, Z. Ahmed, J. M. D’Ewart, J. C. Frisch, R. Herbst, C. Liu, L. Ma, L. Ruckman, D. D. Van Winkle, and C. Yu, “Advanced rfsoc readout for space-based superconducting sensor arrays,” in *Millimeter, Submillimeter, and Far-Infrared Detectors and Instrumentation for Astronomy XI*, Vol. 12190 (SPIE, 2022) pp. 339–355.
- ⁷C. Liu, Z. Ahmed, S. W. Henderson, R. Herbst, and L. Ruckman, “Higher order nyquist zone sampling with rfsoc data converters for astronomical and high energy physics readout systems,” arXiv preprint arXiv:2309.08640 (2023).
- ⁸C. Liu, Z. Ahmed, S. W. Henderson, R. Herbst, L. Ruckman, and T. Satterthwaite, “Development of rfsoc-based direct sampling highly multiplexed microwave squid readout for future cmb and submillimeter surveys,” arXiv preprint arXiv:2406.13156 (2024).
- ⁹M. Bai *et al.*, “C³: A “Cool” Route to the Higgs Boson and Beyond,” in *Snowmass 2021* (2021) arXiv:2110.15800 [hep-ex].
- ¹⁰C. Vernieri *et al.*, “Strategy for Understanding the Higgs Physics: The Cool Copper Collider,” *JINST* **18**, P07053 (2023), arXiv:2203.07646 [hep-ex].
- ¹¹E. A. Nanni, M. Breidenbach, Z. Li, C. Vernieri, F. Wang, G. White, M. Bai, S. Belomestnykh, P. Bhat, T. Barklow, *et al.*, “Status and future plans for c3 r&d,” *Journal of Instrumentation* **18**, P09040 (2023).
- ¹²C. Liu, R. Herbst, B. Hong, L. Ruckman, and E. Nanni, “Direct rf sampling based llrf control system for c-band linear accelerator,” *Proc. IPAC’24*, 25–28 (2024).
- ¹³C. Liu, R. Herbst, L. Ruckman, and E. Nanni, “Next generation llrf control platform for compact c-band linear accelerator,” arXiv (2024), 2407.18198 [physics.acc-ph].
- ¹⁴Z. Geng, “Rf control optimization and automation for normal conducting linear accelerators,” *IEEE Transactions on Nuclear Science* **64**, 2361–2368 (2017).
- ¹⁵SLAC, “Welcome to rogue’s documentation!” Published on Rogue Documentation website <https://slaclab.github.io/rogue/>, (Accessed: 11 August 2024).
- ¹⁶EPICS, “Pv access repositories overview,” Published on EPICS Documentation website <https://docs.epics-controls.org/en/latest/pv-access/overview.html>, (Accessed: 11 August 2024).